

Constraining the Higgs potential using multi-Higgs production

Jia-Le Ding¹, Zach Gillis², Ulrich Haisch^{3*}, Brian Moser⁴, Hai Tao Li¹, Davide Pagani^{5†}, Luca Rottoli⁶, Ambresh Shivaji⁷, Zong-Guo Si¹, Jian Wang^{1‡}, Philipp Windischhofer^{2,8}, Xiao Zhang¹, and Dan Zhao¹

¹ School of Physics, Shandong University, Jinan, Shandong 250100, China

² Department of Physics and Enrico Fermi Institute, University of Chicago, Chicago, IL 60637, USA

³ Max Planck Institute for Physics, Boltzmannstr.8, 85748 Garching, Germany

⁴ Physikalisches Institut, Universität Freiburg, Hermann-Herder Str. 3a, 79104 Freiburg, Germany

⁵ INFN, Sezione di Bologna, Via Irnerio 46, Bologna, I-40126, Italy

⁶ Dipartimento di Fisica G. Occhialini, Università degli Studi di Milano-Bicocca and INFN, Sezione di Milano-Bicocca, Piazza della Scienza, 3, 20126 Milano, Italy

⁷ Indian Institute of Science Education and Research, Knowledge City, Sector 81, S. A. S. Nagar, Manauli PO 140306, Punjab, India

⁸ Kavli Institute for Cosmological Physics, University of Chicago, Chicago, IL 60637, USA

* haisch@mpp.mpg.de, † davide.pagani@bo.infn.it ‡ j.wang@sdu.edu.cn

Preprint: LHCHWG-2025-015, MPP-2025-231

Abstract

The Higgs self-couplings remain only weakly constrained by current Large Hadron Collider (LHC) measurements, leaving ample room for physics beyond the Standard Model that could modify the structure of the Higgs potential. Multi-Higgs production processes provide a particularly sensitive probe of deviations in both the Higgs trilinear and quartic self-couplings. In this note, we summarize the current status of next-to-leading-order electroweak (EW) corrections to double-Higgs production computed within the Standard Model Effective Field Theory and Higgs Effective Field Theory frameworks, emphasizing how these calculations introduce sensitivity to the Higgs self-couplings beyond what is accessible at leading order. We discuss the key conceptual and technical differences between the two effective field theory approaches, including their treatment of higher-dimensional operators, renormalization procedures, and the structure of EW two-loop amplitudes. Despite these differences, both approaches yield broadly consistent constraints, illustrating the complementarity of double- and triple-Higgs measurements. With the high-luminosity LHC and future high-energy colliders on the horizon, these developments and further advances provide an essential foundation for extracting increasingly precise information on the dynamics of EW symmetry breaking.

Copyright attribution to authors.

This work is a submission to SciPost Physics.

License information to appear upon publication.

Publication information to appear upon publication.

Received Date

Accepted Date

Published Date

Contents

1	Introduction	2
2	Constraining the Higgs potential in the SMEFT	4
3	Constraining the Higgs potential in the HEFT	8
4	Conclusions	15
A	Higgs self-couplings and SMEFT operator truncation	16
B	Numerical comparison of SMEFT and HEFT predictions	19
	References	20

1 Introduction

The discovery of the Higgs boson [1, 2] stands as a major milestone in particle physics. Achieving precise measurements of its couplings remains a central objective at the Large Hadron Collider (LHC) and future collider facilities. Compared with the Higgs couplings to electroweak (EW) gauge bosons or third-generation fermions, its self-couplings remain weakly bounded by measurements. Consequently, determining the Higgs trilinear and quartic self-couplings has become a central goal of the long-term physics program at high-energy collider experiments, attracting significant effort from both the experimental and theoretical particle-physics communities.

In the Standard Model (SM), the purely bosonic sector is described by the Lagrangian

$$\mathcal{L} = (D_\mu \phi)^\dagger (D^\mu \phi) + \mu^2 (\phi^\dagger \phi) - \lambda (\phi^\dagger \phi)^2, \quad (1)$$

where the Higgs field ϕ is an $SU(2)_L$ doublet, and D_μ denotes the covariant derivative. The coefficient μ^2 of the quadratic term is chosen to be positive so that the EW symmetry is spontaneously broken. After symmetry breaking, the Higgs field can be written in the unitary gauge as

$$\phi = \frac{1}{\sqrt{2}} \begin{pmatrix} 0 \\ v + H \end{pmatrix}. \quad (2)$$

Here, $v = \sqrt{\mu^2/\lambda} \simeq 246$ GeV is the vacuum expectation value (VEV) of the Higgs field, and H denotes the physical Higgs boson. In the broken phase the Lagrangian (1) takes the form

$$\mathcal{L} \supset m_W^2 W_\mu^+ W^{-\mu} + \frac{1}{2} m_Z^2 Z_\mu Z^\mu - \frac{1}{2} m_H^2 H^2 - v\lambda H^3 - \frac{\lambda}{4} H^4, \quad (3)$$

where the kinetic terms of the Higgs and EW bosons, as well as the interaction terms between the Higgs and the EW gauge bosons, have been omitted for simplicity.

In terms of the fundamental parameters of the SM Lagrangian, the EW gauge boson and Higgs masses are expressed as

$$m_W = \frac{g_2 v}{2}, \quad m_Z = \frac{\sqrt{g_1^2 + g_2^2} v}{2}, \quad m_H = \sqrt{2\lambda} v. \quad (4)$$

Here, g_1 and g_2 denote the gauge couplings of $U(1)_Y$ and $SU(2)_L$, respectively. Once these couplings are fixed by measurements of the W - and Z -boson interactions with the SM fermions, the measured masses of the W , Z , and Higgs bosons are sufficient to fully determine the Lagrangian (3) and, in turn, all purely bosonic interactions of the SM. In particular, the values of m_W and/or m_Z can be used to determine the Higgs vacuum expectation value v , and a measurement of m_H then fixes the quartic coupling λ . This also fixes the dimensionless Higgs trilinear and quartic self-couplings to their SM values

$$\lambda_3^{\text{SM}} = \lambda, \quad \lambda_4^{\text{SM}} = \frac{\lambda}{4}. \quad (5)$$

Notice also that the Lagrangian (3) contains no quintic or higher-order Higgs self-couplings, due to the renormalizability of the Lagrangian (1), which allows at most a quartic $(\phi^\dagger \phi)^2$ term. In view of this feature as well as Eqs. (5), probing the structure of the Higgs potential and the dynamics of EW symmetry breaking provides a stringent test of the consistency of the SM. Any observed deviation from the SM prediction could signal the presence of new physics, such as extended scalar sectors, composite Higgs scenarios, or early-universe phenomena like EW baryogenesis. A broad overview of such beyond-the-SM (BSM) theories can be found, for example, in Refs. [3, 4].

At the LHC, double-Higgs production provides a direct probe of the Higgs trilinear self-coupling, while loop-induced corrections to single-Higgs production and decay processes [5–13] offer complementary indirect constraints. Indeed, both the ATLAS and CMS collaborations have already placed constraints on the Higgs trilinear self-coupling using inclusive measurements of these two classes of processes, based on the complete $\sqrt{s} = 13$ TeV dataset corresponding to approximately 140 fb^{-1} of integrated luminosity [14, 15]. If interpreted in the κ -framework [16–18], which parameterizes modifications of the generalized Higgs trilinear self-coupling $-\nu\lambda_3 H^3$ by

$$\kappa_3 = \frac{\lambda_3}{\lambda_3^{\text{SM}}}, \quad (6)$$

with λ_3^{SM} defined in Eqs. (5), and assuming that all other Higgs couplings take their SM values, the resulting 95% confidence level (CL) bound on κ_3 is [19]

$$-0.71 < \kappa_3 < 6.1. \quad (7)$$

The high-luminosity LHC (HL-LHC) is expected to improve the existing bounds significantly, with the latest combined ATLAS and CMS projection based on a dataset of 6 ab^{-1} reporting the 95% CL limit $0.5 < \kappa_3 < 1.7$ [20]. This hypothetical bound again assumes that all other Higgs couplings take their SM values. Furthermore, since it is derived from theoretical predictions that do not include next-to-leading order (NLO) EW corrections, it is insensitive to the value of the Higgs quartic self-coupling.

Constraining the generalized Higgs quartic self-coupling $-\lambda_4 H^4$, or equivalently

$$\kappa_4 = \frac{\lambda_4}{\lambda_4^{\text{SM}}}, \quad (8)$$

with λ_4^{SM} defined in Eqs. (5), is, compared to the already challenging collider tests of κ_3 , much more difficult. While triple-Higgs production provides a direct probe of the Higgs quartic self-coupling, the tiny triple-Higgs production cross section of about 0.11 fb at $\sqrt{s} = 14 \text{ TeV}$ — roughly 300 times smaller than the double-Higgs production cross section of approximately 36 fb — makes measuring or constraining κ_4 extremely challenging. Given these challenges, experimental constraints on κ_4 did not exist until recently. This has changed with

the first searches for triple-Higgs production conducted by the ATLAS [21] and CMS [22] collaborations. Under the assumption that all other Higgs couplings take their SM values, in particular $\kappa_3 = 1$, the resulting bounds on κ_4 are

$$-230 < \kappa_4 < 240 \quad (\text{ATLAS}), \quad -190 < \kappa_4 < 190 \quad (\text{CMS}), \quad (9)$$

at 95% CL. Under the same assumptions used to obtain Eq. (9), we derive in Section 2 a projected HL-LHC constraint of $-81 < \kappa_4 < 89$, assuming an integrated luminosity of 6 ab^{-1} .

Given the very loose limits on κ_4 , one naturally wonders whether relevant constraints on the Higgs quartic self-coupling can also be obtained from other Higgs production processes once higher-order EW corrections are included. An obvious candidate is double-Higgs production, where two-loop EW corrections introduce a sensitivity to the Higgs quartic self-coupling. In fact, using effective field theories (EFTs), three independent groups [23–25] have computed such effects.¹ The first two works [23, 24] employ the SM Effective Field Theory (SMEFT), while the third [25] uses the Higgs Effective Field Theory (HEFT) framework. The main goal of this note is to summarize and compare the key findings of these publications. To this end, we provide a brief description of the SMEFT calculations [23, 24] of the κ_3 and κ_4 dependence of double-Higgs production in gluon-gluon fusion (ggF), including NLO QCD and EW effects in Section 2, while Section 3 offers a more detailed description of the corresponding HEFT computation [25], its extension to double-Higgs production in vector-boson fusion (VBF), and their phenomenological implications. We conclude in Section 4, where we discuss the conceptual differences between the two calculational frameworks and their model dependence. The complementarity of double- and triple-Higgs production in constraining the Higgs potential is also emphasized. Supplementary material is provided in Appendix A and Appendix B.

2 Constraining the Higgs potential in the SMEFT²

After EW symmetry breaking, the Higgs field H exhibits non-derivative self-interactions, which can be parametrized in a model-independent form as

$$V = \frac{1}{2} m_H^2 H^2 + \kappa_3 \lambda v H^3 + \kappa_4 \frac{\lambda}{4} H^4 + \sum_{n=5}^{\infty} \kappa_n \frac{\lambda}{v^{n-4}} H^n, \quad (10)$$

where κ_3 and κ_4 are defined as in Eqs. (5), (6), and (8). The normalization in Eq. (10) is chosen such that in the SM, one has $\kappa_3 = \kappa_4 = 1$, and $\kappa_n = 0$ for all $n \geq 5$. As explained in the introduction, although constraints on κ_3 are expected to improve substantially with double-Higgs production data at the HL-LHC, placing direct bounds on the Higgs quartic self-coupling modifier κ_4 through measurements of triple-Higgs production remains exceptionally challenging at both future hadron and lepton colliders [23, 24, 34–41].

Prompted by this observation, Refs. [23, 24] evaluated the NLO EW corrections induced by the Higgs self-couplings to double-Higgs production through ggF, taking into account the coupling modifiers κ_3 , κ_4 , and κ_5 . Both calculations make use of the relation

$$\kappa_5 = \frac{7}{4} - \frac{9}{4} \kappa_3 + \frac{1}{2} \kappa_4, \quad (11)$$

which is derived under the assumption that, within the SMEFT framework

$$\mathcal{L}_{\text{SMEFT}} \supset \frac{C_6}{\Lambda^2} Q_6 + \frac{C_8}{\Lambda^4} Q_8, \quad (12)$$

¹Two-loop EW corrections in the SM have been discussed in Refs. [26–33].

²Section authors: Zach Gillis, Ulrich Haisch, Davide Pagani, Brian Moser, Luca Rottoli, Ambresh Shivaji, and Philipp Windischhofer.

only the dimension-six and dimension-eight operators

$$Q_6 = (\phi^\dagger \phi)^3, \quad Q_8 = (\phi^\dagger \phi)^4, \quad (13)$$

contribute to modifications of the Higgs self-couplings, while other possible operators, such as the dimension-ten operator $Q_{10} = (\phi^\dagger \phi)^5$, are assumed to have no effect. In Eq. (12), the symbol Λ denotes the scale of new physics that suppresses the higher-dimensional operators Q_6 and Q_8 , rendering their Wilson coefficients C_6 and C_8 dimensionless. In Appendix A, we show that restricting the SMEFT Lagrangian to operators of the form $(\phi^\dagger \phi)^n$, as in Eq. (12), provides a good approximation for BSM models that primarily modify the Higgs self-couplings, while inducing only minor effects on other SMEFT operators. Strictly speaking, the phenomenological analysis below therefore applies only to such models. These scenarios are, however, particularly interesting, as probing the Higgs self-couplings via multi-Higgs production at the HL-LHC and future colliders explores largely uncharted parameter space, offering genuine discovery potential even if single-Higgs observables appear SM-like.

It is important to emphasize that, under the above assumption, a one-to-one correspondence exists between the coupling modifiers κ_3 and κ_4 and the Wilson coefficients C_6 and C_8 introduced in Eq. (12). This mapping is explicitly given by

$$\begin{aligned} C_6 &= -\frac{2m_h^2 \Lambda^2}{v^4} (\kappa_3 - 1) + \frac{m_h^2 \Lambda^2}{4v^4} (\kappa_4 - 1), \\ C_8 &= \frac{3m_h^2 \Lambda^4}{4v^6} (\kappa_3 - 1) - \frac{m_h^2 \Lambda^4}{8v^6} (\kappa_4 - 1). \end{aligned} \quad (14)$$

In the following, all formulas, constraints, and limits in this section are expressed in terms of κ_3 and κ_4 . Alternatively, one may work with C_6 and C_8 , using the correspondence given in Eqs. (14).

Employing Eqs. (11) and (12), Ref. [23] computed the NLO EW corrections to the $gg \rightarrow HH$ amplitudes at $\mathcal{O}(\kappa_4)$ and $\mathcal{O}(\kappa_3 \kappa_4)$, while the computation in Ref. [24] additionally includes contributions at $\mathcal{O}(\kappa_3^2)$ and $\mathcal{O}(\kappa_3^3)$. Subsequently, NLO EW corrections involving κ_3 and κ_4 have been computed within the HEFT framework [25]. Details of this calculation are provided in Section 3. The corrections computed in Ref. [23] have been incorporated into the POWHEG BOX framework [42], where they are combined with NLO QCD corrections that account for κ_3 variations, including the full top-quark mass effects [43–47]. As shown in Ref. [48], the POWHEG BOX implementation accurately reproduces the LHC Higgs Cross Section Working Group’s current recommendations for the double-Higgs production cross section as a function of κ_3 , based on Refs. [49, 50], which carry relative uncertainties of about $\pm 15\%$ arising from the choice of the renormalization and top-quark mass schemes [51].

The POWHEG BOX implementation described above enables an efficient computation of the inclusive $gg \rightarrow HH$ production cross section at the LHC. Using the PDF4LHC15_NLO parton distribution functions (PDFs) [52],³ with $m_t = 173$ GeV and adopting the scale choice $\mu_R = \mu_F = m_{HH}/2$ — where m_t denotes the top-quark mass, μ_R and μ_F represent the renormalization and factorization scales, respectively, and m_{HH} is the invariant mass of the final-state Higgs pair — the following signal strengths for collisions at $\sqrt{s} = 13$ TeV, $\sqrt{s} = 13.6$ TeV,

³The specific choice of PDFs has only a very minor numerical impact on all the formulas and results presented in this and the following section.

and $\sqrt{s} = 14 \text{ TeV}$ are obtained [48]:

$$\begin{aligned}
\mu_{2h,\text{SMEFT}}^{13 \text{ TeV}} &= 2.21 - 1.54\kappa_3 - 1.04 \cdot 10^{-3}\kappa_4 + 3.35 \cdot 10^{-1}\kappa_3^2 + 4.06 \cdot 10^{-3}\kappa_3\kappa_4 \\
&\quad + 5.59 \cdot 10^{-5}\kappa_4^2 - 1.62 \cdot 10^{-3}\kappa_3^2\kappa_4 - 3.86 \cdot 10^{-5}\kappa_3\kappa_4^2 + 9.82 \cdot 10^{-6}\kappa_3^2\kappa_4^2, \\
\mu_{2h,\text{SMEFT}}^{13.6 \text{ TeV}} &= 2.20 - 1.53\kappa_3 - 1.01 \cdot 10^{-3}\kappa_4 + 3.32 \cdot 10^{-1}\kappa_3^2 + 4.02 \cdot 10^{-3}\kappa_3\kappa_4 \\
&\quad + 5.60 \cdot 10^{-5}\kappa_4^2 - 1.60 \cdot 10^{-3}\kappa_3^2\kappa_4 - 3.85 \cdot 10^{-5}\kappa_3\kappa_4^2 + 9.77 \cdot 10^{-6}\kappa_3^2\kappa_4^2, \\
\mu_{2h,\text{SMEFT}}^{14 \text{ TeV}} &= 2.20 - 1.53\kappa_3 - 0.98 \cdot 10^{-3}\kappa_4 + 3.30 \cdot 10^{-1}\kappa_3^2 + 4.00 \cdot 10^{-3}\kappa_3\kappa_4 \\
&\quad + 5.60 \cdot 10^{-5}\kappa_4^2 - 1.59 \cdot 10^{-3}\kappa_3^2\kappa_4 - 3.84 \cdot 10^{-5}\kappa_3\kappa_4^2 + 9.74 \cdot 10^{-6}\kappa_3^2\kappa_4^2.
\end{aligned} \tag{15}$$

Three features of the above expressions are worth highlighting. First, each power of κ_4 introduces a relative suppression of $\mathcal{O}(10^{-3})$, reflecting the fact that κ_4 contributions enter only at NLO, whereas the leading κ_3 dependence appears already at leading order (LO) in EW interactions. Second, the different coefficients show only a very weak dependence on \sqrt{s} across the range of center-of-mass (CM) energies considered. Additional expressions analogous to Eqs. (15), corresponding to different scale choices at the LHC and relevant to the hadron mode of the Future Circular Collider (FCC-hh), can be found in Refs. [48, 53]. Using the results of Ref. [53], one can also include next-to-next-to-leading order (NNLO) EW corrections in Eqs. (15), arising from two-loop contributions to the wave function renormalization constant of the Higgs field. These corrections generally have a limited numerical impact. For example, in the case of the κ_4^2 coefficients, NNLO EW effects due to the Higgs wave function renormalization correspond to a relative shift of about 20%. The same NNLO EW effects from Higgs wave function renormalization also induce a dependence of all single-Higgs production processes on κ_4 . However, since these effects first arise at three loops, the resulting sensitivity to κ_4 is very limited [53].

The two panels in Figure 1 present the results of a sensitivity analysis for constraining κ_3 and κ_4 , based on both existing LHC Run 2 data and projections for the HL-LHC with an assumed integrated luminosity of 3 ab^{-1} . The red and green contours indicate the 68% CL limits derived from double- and triple-Higgs production, respectively. Constraints from double-Higgs production are obtained using Eqs. (15), while those from triple-Higgs production are computed at LO in QCD using MadGraph5_aMC@NLO [54], with NLO QCD corrections from Ref. [55] included as an overall normalization factor. Expressions for signal strengths in triple-Higgs production, analogous to Eqs. (15), can be found in Refs. [23, 53]. The double- and triple-Higgs constraints shown for LHC Run 2 assume $\mu_{2h}^{\text{LHC Run 2}} < 2.9$ [56] and $\mu_{3h}^{\text{LHC Run 2}} < 588$ [22], while at the HL-LHC we have assumed that the corresponding signal strengths can be constrained to $0.77 < \mu_{2h}^{\text{HL-LHC}} < 1.23$ and $\mu_{3h}^{\text{HL-LHC}} < 125$. These hypothetical limits are consistent with those derived in Ref. [57] and Ref. [58], respectively. The SM prediction is marked by the black dots, while the dashed black lines represent the set of solutions satisfying $\kappa_4 - 1 = 6(\kappa_3 - 1)$. This relation holds under the assumption that Q_6 in Eqs. (12) is the only SMEFT operator with a non-zero Wilson coefficient.

The results shown in the figure clearly demonstrate that, at the LHC, the constraints from double- and triple-Higgs production are largely complementary. Double-Higgs production is primarily sensitive to variations in κ_3 , whereas triple-Higgs production generally yields stronger bounds on κ_4 . This observation has also been made in Refs. [23–25, 48, 53]. Assuming $\kappa_3 = 1$, our analysis yields the 95% CL constraint

$$-185 < \kappa_4 < 193, \tag{16}$$

consistent with the limits reported by the ATLAS and CMS collaborations in Refs. [21, 22] and quoted in Eqs. (9). Our HL-LHC projection, assuming an integrated luminosity of 6 ab^{-1} ,

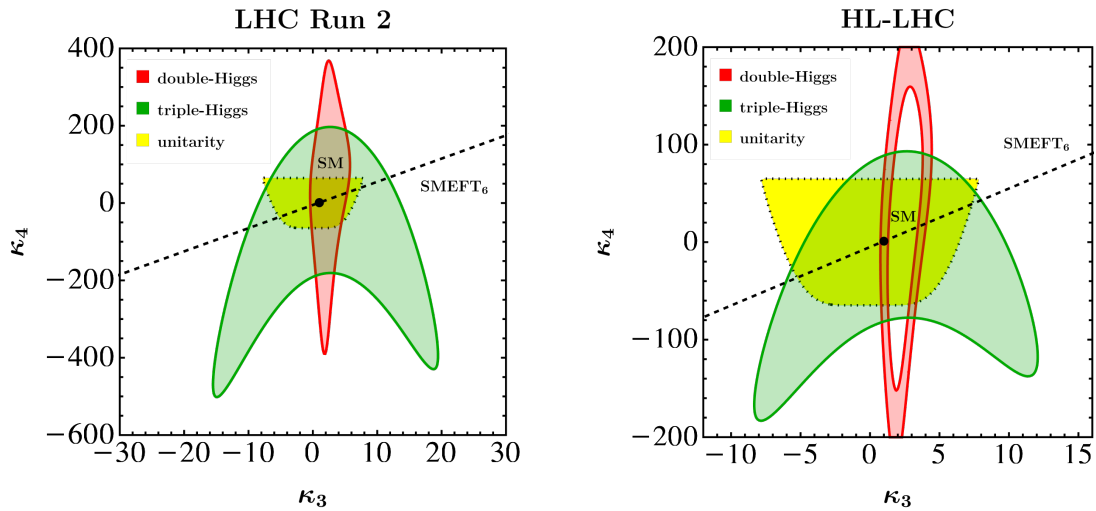


Figure 1: Constraints in the κ_3 - κ_4 plane at the LHC Run 2 (left) and the HL-LHC (right). The red and green contours correspond to the preferred 68% CL regions that arise from inclusive double- and triple-Higgs production, respectively. The SM is indicated by the black points, and the black dashed lines correspond to $\kappa_4 - 1 = 6(\kappa_3 - 1)$, i.e., the relation between κ_3 and κ_4 that holds in the SMEFT at the level of dimension-six operators. The yellow regions, outlined with black dotted lines, indicate the constraint from perturbative unitarity derived from tree-level $HH \rightarrow HH$ scattering.

reduces the allowed 95% CL range to

$$-81 < \kappa_4 < 89, \quad (17)$$

comparable to the limits set by perturbative unitarity [35, 38, 59], depicted as a yellow region with a black dotted outline in both panels of Figure 1. Improvements in background uncertainties and b -tagging performance relative to the LHC Run 2 baseline could further strengthen the bound given in Eq. (17). We have confirmed that, within this region, the two NLO EW computations of double-Higgs production [23, 24] yield numerically similar constraints in the κ_3 - κ_4 plane.⁴ Based on perturbativity considerations [34, 59], the calculation in Ref. [24] is valid only within the range $-4 \lesssim \kappa_3 \lesssim 6$ and $6\kappa_3 - 36 \lesssim \kappa_4 \lesssim 6\kappa_3 + 26$. Although this region is not shown in Figure 1, it encompasses the overlap of the red and yellow areas corresponding to constraints from double-Higgs production and unitarity, respectively. Importantly, if only the value of the total cross section of double-Higgs production is taken into account, two distinct regions in parameter space are likely to remain allowed, with one centered around the SM point and the other near $\{\kappa_3, \kappa_4\} \simeq \{3.5, 16\}$. Note that the LHC Run 2 analysis exhibits the same BSM solutions, but they are not resolved because the double-Higgs signal strength is only bounded from above, $\mu_2^{\text{LHC Run 2}} < 2.9$. At the HL-LHC, with $0.77 < \mu_{2h}^{\text{HL-LHC}} < 1.23$, and since Eqs. (15) are polynomial in κ_3 and κ_4 , this produces an elongated ellipsoidal band rather than a closed contour. Furthermore, observe that this BSM solution is consistent with the κ_3 bound quoted after Eqs. (7) from ATLAS and CMS projections. In addition to the total cross section, these projections incorporate differential information via Monte Carlo (MC) simulations, enabling them to break the degeneracy and favor values near the SM point. We also notice that even at the HL-LHC the total cross section alone will not suffice to distinguish between BSM scenarios in which deviations in Higgs self-interactions arise exclusively from the

⁴Since the two computations include different subsets of NLO EW corrections induced by the Higgs self-couplings, a detailed comparison is non-trivial and is therefore deferred to future work.

SMEFT operator Q_6 , or from a combination of the operators Q_6 and Q_8 as defined in Eqs. (13). On the other hand, incorporating kinematic information in double-Higgs production could affect this conclusion — see Section 3. As shown in Refs. [23, 53], the FCC-hh would be able to resolve the degeneracy depicted in the right plot in Figure 1.

3 Constraining the Higgs potential in the HEFT⁵

Before discussing in some detail the calculation of the NLO EW corrections to double-Higgs production in the HEFT, it is useful to comment on the impact of QCD corrections on the extraction of κ_3 from double-Higgs production measurements. Keeping the κ_3 dependence, the LO cross section for double-Higgs production via ggF can be written as

$$\sigma_{\text{ggF,LO}}^{\sqrt{s}} = (\sigma_{\text{ggF,LO}}^{\sqrt{s}})_{\text{SM}} \left(1 - 0.81(\kappa_3 - 1) + 0.28(\kappa_3 - 1)^2 \right), \quad (18)$$

where

$$(\sigma_{\text{ggF,LO}}^{13 \text{ TeV}})_{\text{SM}} = 16.7 \text{ fb}, \quad (\sigma_{\text{ggF,LO}}^{13.6 \text{ TeV}})_{\text{SM}} = 18.6 \text{ fb}, \quad (\sigma_{\text{ggF,LO}}^{14 \text{ TeV}})_{\text{SM}} = 19.8 \text{ fb}, \quad (19)$$

are the LO SM cross-section predictions at the corresponding CM energies. Higher-order QCD corrections do not alter the polynomial structure of these expressions, but only modify the coefficients. For the corresponding NLO QCD cross sections, we find

$$\sigma_{\text{ggF,NLO}}^{\sqrt{s}} = (\sigma_{\text{ggF,NLO}}^{\sqrt{s}})_{\text{SM}} \left(1 - 0.87(\kappa_3 - 1) + 0.33(\kappa_3 - 1)^2 \right), \quad (20)$$

where

$$(\sigma_{\text{ggF,NLO}}^{13 \text{ TeV}})_{\text{SM}} = 27.8 \text{ fb}, \quad (\sigma_{\text{ggF,NLO}}^{13.6 \text{ TeV}})_{\text{SM}} = 30.8 \text{ fb}, \quad (\sigma_{\text{ggF,NLO}}^{14 \text{ TeV}})_{\text{SM}} = 33.0 \text{ fb}. \quad (21)$$

These NLO QCD predictions were obtained using the two-loop $gg \rightarrow HH$ amplitude [43] as implemented in the POWHEG BOX, while the one-loop amplitudes for $gg \rightarrow HHg$ and other related partonic processes were generated with OpenLoops [60, 61]. Infrared divergences are treated using the dipole subtraction method [62, 63]. The NLO QCD results have also been cross-checked by means of the ggxy program [64, 66]. The following comment concerning Eqs. (18) and (20) is in order. We find that the κ_3 dependence is essentially independent of \sqrt{s} at each perturbative order in QCD. However, the κ_3 dependence does change when going from LO to NLO in QCD, with the linear and quadratic terms in κ_3 being modified differently. While the linear term receives a relative correction of about +7%, the quadratic term is shifted by approximately +18%. Including QCD corrections therefore enhances the sensitivity to modifications of the Higgs trilinear self-coupling, making it important to account for them when interpreting LHC data on ggF double-Higgs production.

Compared to the ggF channel, the impact of QCD corrections is much less pronounced in

⁵Section authors: Jia-Le Ding, Hai Tao Li, Zong-Guo Si, Jian Wang, Xiao Zhang, and Dan Zhao.

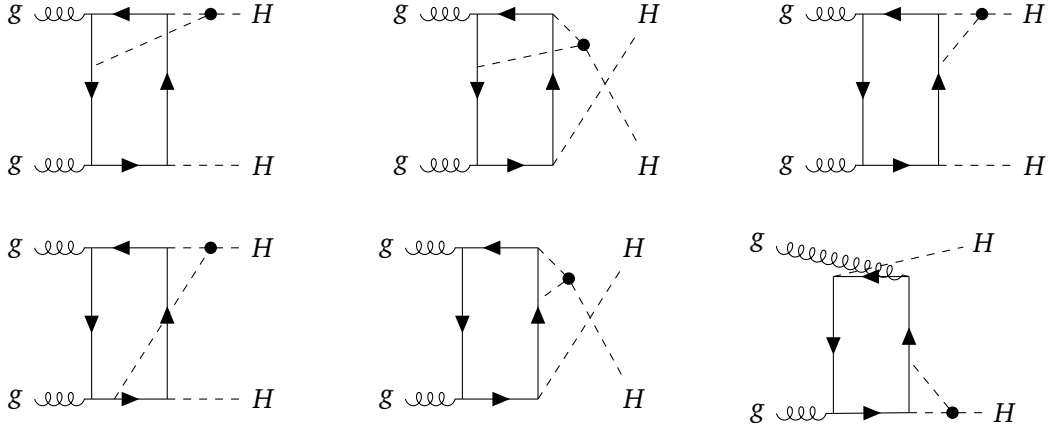


Figure 2: Feynman diagrams contributing to $gg \rightarrow HH$ that contain a single Higgs trilinear self-coupling (black dot) and three top-quark Yukawa couplings. The diagrams with reversed fermion flow are omitted.

VBF double-Higgs production. We obtain

$$\begin{aligned}
\sigma_{\text{VBF,LO}}^{13\text{TeV}} &= 1.71 \left(1 - 0.91(\kappa_3 - 1) + 0.73(\kappa_3 - 1)^2 \right) \text{fb}, \\
\sigma_{\text{VBF,LO}}^{13.6\text{TeV}} &= 1.90 \left(1 - 0.89(\kappa_3 - 1) + 0.72(\kappa_3 - 1)^2 \right) \text{fb}, \\
\sigma_{\text{VBF,LO}}^{14\text{TeV}} &= 2.03 \left(1 - 0.90(\kappa_3 - 1) + 0.71(\kappa_3 - 1)^2 \right) \text{fb}, \\
\sigma_{\text{VBF,N}^3\text{LO}}^{13\text{TeV}} &= 1.70 \left(1 - 0.89(\kappa_3 - 1) + 0.72(\kappa_3 - 1)^2 \right) \text{fb}, \\
\sigma_{\text{VBF,N}^3\text{LO}}^{13.6\text{TeV}} &= 1.89 \left(1 - 0.88(\kappa_3 - 1) + 0.71(\kappa_3 - 1)^2 \right) \text{fb}, \\
\sigma_{\text{VBF,N}^3\text{LO}}^{14\text{TeV}} &= 2.01 \left(1 - 0.88(\kappa_3 - 1) + 0.71(\kappa_3 - 1)^2 \right) \text{fb}.
\end{aligned} \tag{22}$$

One observes that the inclusion of next-to-next-to-next-to-leading order (N^3LO) QCD corrections reduces the SM cross sections by about -1% at each CM energy, leaving the κ_3 dependence essentially unchanged. This is expected from the factorization properties of VBF-like processes, which can be accurately treated as two independent deep-inelastic scattering processes using the structure function approach. The effect of non-factorizable NNLO QCD corrections associated with κ_3 in VBF double-Higgs production was studied in Ref. [65] and found to be at most approximately -0.35% for $-2 < \kappa_3 < 4$.

The NLO EW corrections to double-Higgs production involving κ_3 and κ_4 can be computed within the HEFT framework, using the EW chiral Lagrangian, which can be regarded as an extension of the κ -framework to a fully consistent quantum field theory. At the LO the EW chiral Lagrangian is given by [67]

$$\mathcal{L}_2 = \frac{1}{2} (\partial_\mu H)(\partial^\mu H) - T - V + \frac{v^2}{4} \left(1 + 2c_1 \frac{H}{v} + c_2 \left(\frac{H}{v} \right)^2 + \dots \right) \text{Tr} [D_\mu U^\dagger D^\mu U] + \dots, \tag{23}$$

where we have written the Higgs potential V and the interaction terms between the Higgs boson and the EW gauge bosons explicitly, assuming that the fermionic sector remains the same as in the SM. The matrix U parameterizes the Goldstone bosons π^k nonlinearly,

$$U = e^{\frac{i\pi^k \sigma^k}{v}}, \tag{24}$$

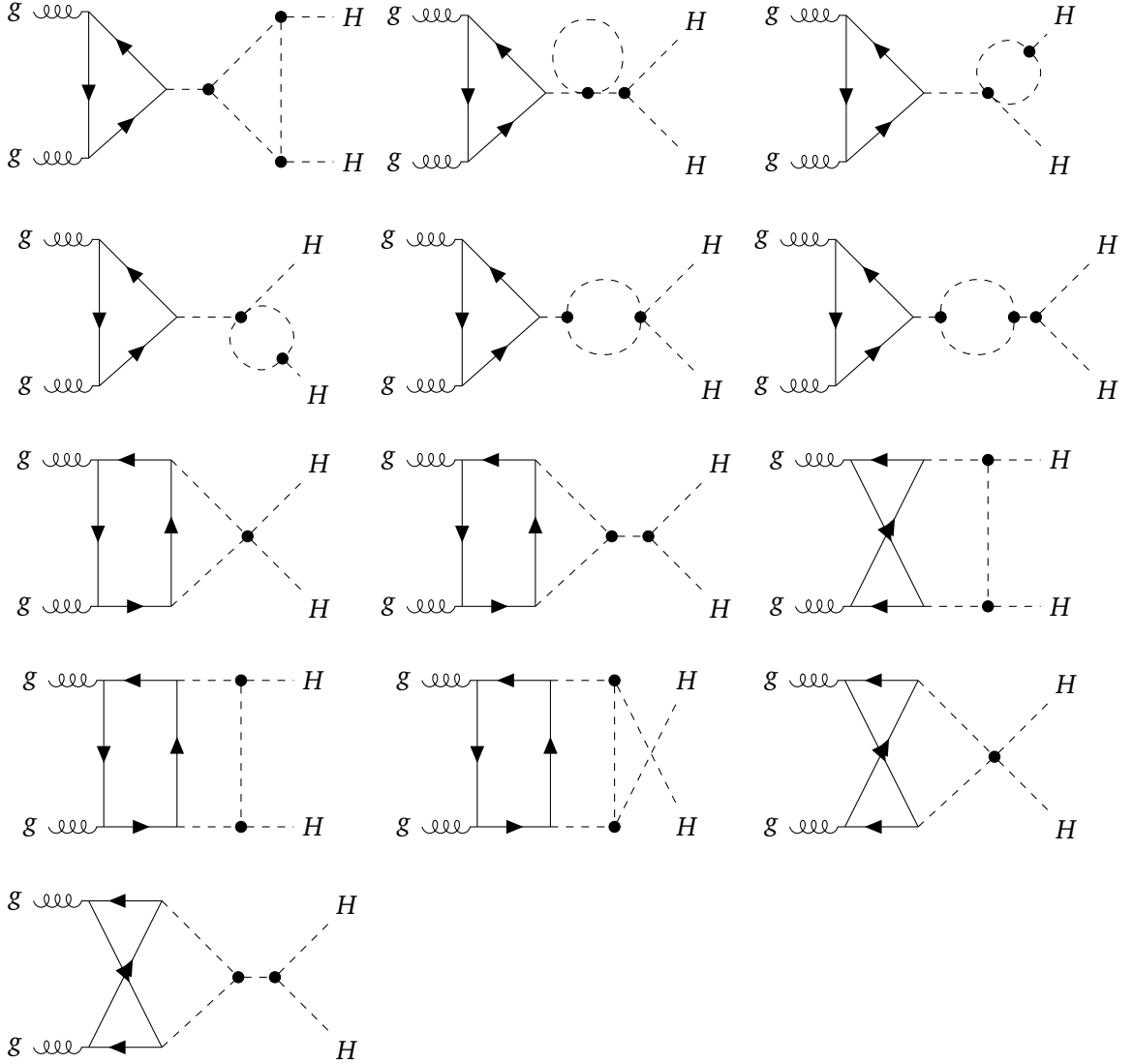


Figure 3: Feynman diagrams contributing to $gg \rightarrow HH$ that contain at least two Higgs trilinear self-couplings or a single Higgs quartic self-coupling. The modified Higgs self-interactions are indicated by black dots. The diagrams with reversed fermion flow are omitted.

where σ^k are the Pauli matrices and $k = 1, 2, 3$. The covariant derivative acting on U is defined as

$$D_\mu U = \partial_\mu U + ig_2 W_\mu^k \frac{\sigma^k}{2} U - ig_1 B_\mu U \frac{\sigma^3}{2}. \quad (25)$$

Here, W_μ^k and B_μ denote the $SU(2)_L$ and $U(1)_Y$ gauge fields, respectively. The factor $v^2/4$ in Eq. (23) is chosen to reproduce the correct masses of the EW gauge bosons, while the coefficients c_1 and c_2 parameterize the couplings between the EW gauge bosons and one or two Higgs bosons, respectively. Besides the Higgs potential V given in Eq. (10), the Lagrangian (23) also contains the Higgs tadpole term

$$T = (m_H^2 - 2\lambda v^2) vH. \quad (26)$$

This term vanishes at tree level due to $m_H^2 = 2\lambda v^2$ and has therefore been omitted in many studies based on the EW chiral Lagrangian. However, it is required once the renormalization of

the Higgs field is considered. Note also that the SM Lagrangian (3) is recovered from Eqs. (10), (23), and (26) when $c_1 = c_2 = \kappa_3 = \kappa_4 = 1$ and all $\kappa_n = 0$ for $n \geq 5$.

In the case of double-Higgs production in ggF, there are two types of NLO EW corrections that modify the dependence of the differential cross section on the Higgs self-couplings. The first type arises from diagrams with at most one triple-Higgs vertex. The diagrams which contain a single Higgs trilinear self-coupling and three top-quark Yukawa couplings are shown in Figure 2. These contributions are ultraviolet (UV) finite for the $gg \rightarrow HH$ amplitude, as the Higgs trilinear self-coupling does not mix with the top-quark Yukawa coupling at the one-loop order. This mixing first appears at the two-loop level, giving rise to a non-zero anomalous dimension [5]. The interference of these two-loop diagrams with the LO amplitudes yields the following additive corrections

$$\begin{aligned}\sigma_{\text{ggF,EW}_1}^{13\text{TeV}} &= (-0.176\kappa_3^2 + 0.572\kappa_3)\text{fb}, \\ \sigma_{\text{ggF,EW}_1}^{13.6\text{TeV}} &= (-0.194\kappa_3^2 + 0.632\kappa_3)\text{fb}, \\ \sigma_{\text{ggF,EW}_1}^{14\text{TeV}} &= (-0.207\kappa_3^2 + 0.674\kappa_3)\text{fb},\end{aligned}\tag{27}$$

which exhibit a mild dependence on the collider energy \sqrt{s} . Compared to the NLO QCD corrections (20), these NLO EW effects change the linear (quadratic) κ_3 dependence of the ggF double-Higgs production cross section by about -1% (-2%). Comparable effects are expected from the NLO EW corrections involving the EW gauge bosons, as demonstrated in the case of the SM in Ref. [29].

A second type of NLO EW corrections to double-Higgs production arises from diagrams containing at least two triple-Higgs vertices or a Higgs quartic self-coupling. For the ggF channel, the relevant two-loop diagrams are shown in Figure 3. Given the currently weak bounds on κ_3 and κ_4 in Eqs. (7) and (9), this type of NLO EW contribution can be phenomenologically much larger than the corrections in Eqs. (27). The calculation of this second type of NLO EW corrections requires renormalization of the Higgs sector within the HEFT, as the diagrams in Figure 3 contain UV divergences. To achieve this, we introduce renormalization constants via redefinitions of the fields and parameters:

$$H = Z_H^{1/2} H_R \quad m_H^2 = Z_{m^2} m_{H,R}^2 \quad v = Z_v v_R, \quad \lambda = Z_\lambda \lambda_R \quad \kappa_3 = Z_{\kappa_3} \kappa_{3,R}, \quad \kappa_4 = Z_{\kappa_4} \kappa_{4,R},\tag{28}$$

where the subscript R denotes renormalized quantities. Since the Higgs quartic self-coupling enters only at the two-loop level, the coupling modifier κ_4 does not require renormalization, implying that the corresponding Z factor can be set to one, i.e., $Z_{\kappa_4} = 1$.

Inserting the renormalized quantities (28) back into the Lagrangian (23) yields the following counterterms for the one-, two-, and three-point Higgs vertices:

$$\begin{aligned}\text{---}\otimes\text{---} &= -2i\lambda v^3 (\delta Z_{m^2} - 2\delta Z_v - \delta Z_\lambda), \\ \text{---}\otimes\text{---}\text{---} &= i [p^2 \delta Z_H - (\delta Z_{m^2} + \delta Z_H) m_H^2], \\ \text{---}\otimes\text{---}\text{---} &= -6i\kappa_3 \lambda v \left(\frac{3}{2} \delta Z_H + \delta Z_\lambda + \delta Z_v + \delta Z_{\kappa_3} \right).\end{aligned}\tag{29}$$

Here, we have used the notation $\delta Z = Z - 1$. The renormalization conditions are chosen as follows:

- The Higgs tadpole contribution is renormalized to zero.

- The Higgs mass and wave function are renormalized in the on-shell scheme.
- The coupling modifier κ_3 is renormalized in the $\overline{\text{MS}}$ scheme.

Since the renormalization of the W - and Z -boson masses, as well as the electric charge, does not involve the Higgs trilinear self-coupling at the one-loop level, we can leave the VEV v unrenormalized by setting $\delta Z_v = 0$ without loss of generality. Making use of the above renormalization conditions, the Z factors are uniquely determined. For instance, for the $\overline{\text{MS}}$ counterterm of κ_3 , we obtain

$$\delta Z_{\kappa_3} = \frac{3\lambda}{16\pi^2} \frac{1}{\epsilon} (\kappa_3 + 2\kappa_4 - 3\kappa_3^2), \quad (30)$$

where the UV pole $1/\epsilon$ with $\epsilon = (4-d)/2$ arises from dimensional regularization in d dimensions. The inclusion of the counterterm contributions (29) removes all UV divergences present in the bare two-loop amplitudes.

In the following, we present results for the second type of NLO EW contributions for both ggF and VBF double-Higgs production, which constitute the two dominant double-Higgs production mechanisms at the LHC. Since the two-loop $gg \rightarrow HH$ diagrams involve multiple scales, obtaining analytical results is currently beyond the state-of-the-art. We therefore adopt a numerical approach using the AMFlow package [68, 69]. In contrast, the loop diagrams in the VBF channel are computed analytically and implemented into the proVBFHH program [70–73] to perform MC integrations. To obtain numerical predictions, we use the input parameters

$$\begin{aligned} v &= 246.2 \text{ GeV}, & m_H &= 125 \text{ GeV}, & m_t &= 173 \text{ GeV}, \\ m_W &= 80.379 \text{ GeV}, & m_Z &= 91.1876 \text{ GeV}, \end{aligned} \quad (31)$$

and employ the PDF4LHC15_NLO PDF set together with the associated strong coupling α_s . In the ggF double-Higgs production cross-section calculation, the renormalization and factorization scales are chosen as $\mu_R = \mu_F = m_{HH}/2$, while in the VBF channel we use $\mu_R = \mu_F = \sqrt{-q^2}$, where q^2 denotes the momentum squared transferred in the t -channel exchange between the two quark lines.

The interference between the two-loop diagrams shown in Figure 3, including the corresponding one-loop counterterms, and the LO $gg \rightarrow HH$ amplitudes, yields the following additive contributions to the ggF double-Higgs production cross section:

$$\begin{aligned} \sigma_{\text{ggF,EW}_{\text{II}}}^{13\text{TeV}} &= (0.067\kappa_3^4 - 0.105\kappa_3^3 - 0.006\kappa_3^2\kappa_4 - 0.166\kappa_3^2 + 0.070\kappa_3\kappa_4 - 0.149\kappa_4) \text{ fb}, \\ \sigma_{\text{ggF,EW}_{\text{II}}}^{13.6\text{TeV}} &= (0.074\kappa_3^4 - 0.114\kappa_3^3 - 0.006\kappa_3^2\kappa_4 - 0.185\kappa_3^2 + 0.077\kappa_3\kappa_4 - 0.163\kappa_4) \text{ fb}, \\ \sigma_{\text{ggF,EW}_{\text{II}}}^{14\text{TeV}} &= (0.078\kappa_3^4 - 0.120\kappa_3^3 - 0.006\kappa_3^2\kappa_4 - 0.199\kappa_3^2 + 0.081\kappa_3\kappa_4 - 0.173\kappa_4) \text{ fb}. \end{aligned} \quad (32)$$

The corresponding NLO EW corrections of the second type for VBF double-Higgs production are given by

$$\begin{aligned} \sigma_{\text{VBF,EW}_{\text{II}}}^{13\text{TeV}} &= (1.96\kappa_3^4 - 2.35\kappa_3^3 - 0.14\kappa_3^2\kappa_4 - 1.65\kappa_3^2 + 1.26\kappa_3\kappa_4 - 1.93\kappa_4) \cdot 10^{-2} \text{ fb}, \\ \sigma_{\text{VBF,EW}_{\text{II}}}^{13.6\text{TeV}} &= (2.11\kappa_3^4 - 2.00\kappa_3^3 - 0.44\kappa_3^2\kappa_4 - 3.76\kappa_3^2 + 3.35\kappa_3\kappa_4 - 3.56\kappa_4) \cdot 10^{-2} \text{ fb}, \\ \sigma_{\text{VBF,EW}_{\text{II}}}^{14\text{TeV}} &= (2.27\kappa_3^4 - 2.65\kappa_3^3 - 0.21\kappa_3^2\kappa_4 - 2.16\kappa_3^2 + 1.74\kappa_3\kappa_4 - 2.46\kappa_4) \cdot 10^{-2} \text{ fb}. \end{aligned} \quad (33)$$

The results in Eqs. (33) are obtained under the assumption $c_1 = c_2 = 1$, see Eq. (23). Comparing the ggF and VBF results, one observes that although the cross-section modifications in the VBF channel are generally smaller than in the ggF process, the dependence on κ_3 and κ_4

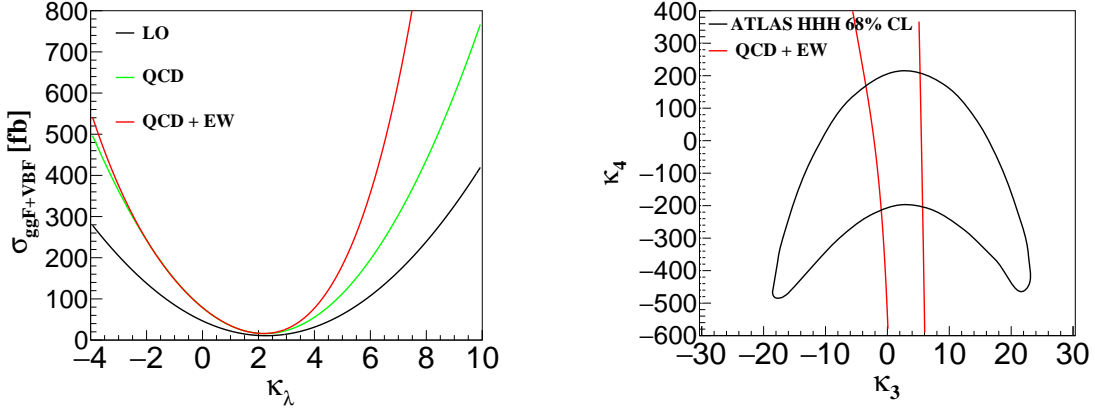


Figure 4: Left: Cross sections for double-Higgs production in the combined ggF and VBF channels at the LHC with $\sqrt{s} = 14$ TeV as a function of $\kappa_\lambda = \kappa_3 = \kappa_4$. The black line shows the LO prediction, the green line includes QCD corrections, and the red line incorporates NLO QCD and NLO EW in ggF and N³LO QCD and NLO EW in VBF, collectively referred to as QCD+EW. Right: Constraints in the $\kappa_3 - \kappa_4$ plane from LHC Run 2. The red contour corresponds to the preferred 68% CL region derived from the HEFT calculation of the QCD+EW corrections to double-Higgs production presented here. For comparison, the 68% CL region from triple-Higgs production, as obtained by the ATLAS collaboration [21], is shown as a black contour.

differs markedly between the two channels. In addition, the \sqrt{s} dependence of the cross sections is more pronounced for VBF than for ggF double-Higgs production. A combination of both channels therefore leads to an improved sensitivity to κ_3 and κ_4 .

Combining the results presented in Eqs. (20), (22), (27), (32), and (33), we obtain the following expressions for the inclusive double-Higgs production signal strengths in the HEFT:

$$\begin{aligned}
\mu_{2h,\text{HEFT}}^{13\text{ TeV}} &= 2.22 - 1.55\kappa_3 - 5.69 \cdot 10^{-3}\kappa_4 + 3.39 \cdot 10^{-1}\kappa_3^2 + 2.79 \cdot 10^{-3}\kappa_3\kappa_4 \\
&\quad - 2.50 \cdot 10^{-4}\kappa_3^2\kappa_4 - 4.34 \cdot 10^{-3}\kappa_3^3 + 2.93 \cdot 10^{-3}\kappa_3^4, \\
\mu_{2h,\text{HEFT}}^{13.6\text{ TeV}} &= 2.22 - 1.55\kappa_3 - 6.06 \cdot 10^{-3}\kappa_4 + 3.38 \cdot 10^{-1}\kappa_3^2 + 3.37 \cdot 10^{-3}\kappa_3\kappa_4 \\
&\quad - 3.17 \cdot 10^{-4}\kappa_3^2\kappa_4 - 4.09 \cdot 10^{-3}\kappa_3^3 + 2.90 \cdot 10^{-3}\kappa_3^4, \\
\mu_{2h,\text{HEFT}}^{14\text{ TeV}} &= 2.22 - 1.55\kappa_3 - 5.63 \cdot 10^{-3}\kappa_4 + 3.39 \cdot 10^{-1}\kappa_3^2 + 2.80 \cdot 10^{-3}\kappa_3\kappa_4 \\
&\quad - 2.31 \cdot 10^{-4}\kappa_3^2\kappa_4 - 4.17 \cdot 10^{-3}\kappa_3^3 + 2.87 \cdot 10^{-3}\kappa_3^4.
\end{aligned} \tag{34}$$

Notice that, unlike Eqs. (15), which consider only ggF double-Higgs production corrections, these expressions include contributions from both the ggF and VBF channels.

In the left plot of Figure 4, we show the cross sections for double-Higgs production in the combined ggF and VBF channels at the LHC with $\sqrt{s} = 14$ TeV as a function of $\kappa_\lambda = \kappa_3 = \kappa_4$ at different perturbative orders in the HEFT. Specifically, the black line corresponds to the LO predictions given in Eqs. (18) and (22), while the green line shows the higher-order QCD predictions from Eqs. (20) and (22). The red line additionally includes the NLO EW effects of Eqs. (27), (32), and (33), assuming that the EW and QCD corrections are factorizable. We first note that, for the considered range of κ_λ , the VBF process contributes between 6% and 19% of the total double-Higgs production cross section. One furthermore observes that for $\kappa_\lambda \gtrsim 3.5$, the NLO EW effects are as important as, or even more important than, the QCD corrections.

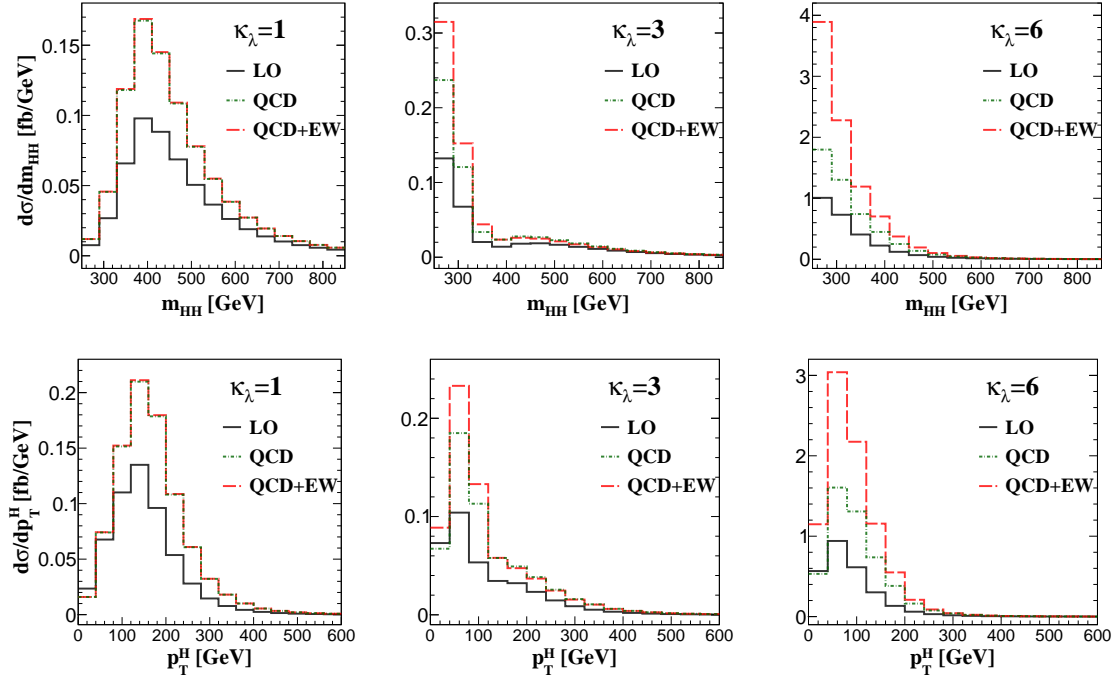


Figure 5: Kinematic distributions for double-Higgs production in the combined ggF and VBF channels at the LHC with $\sqrt{s} = 14$ TeV for three different κ_λ values, assuming $\kappa_\lambda = \kappa_3 = \kappa_4$. The black lines show the LO predictions, the green dash-dotted lines include QCD corrections, and the red dashed lines incorporate both QCD and EW corrections. The upper panels display m_{HH} spectra, while the lower panels show p_T^H distributions.

This is phenomenologically relevant, as incorporating NLO EW effects into the experimental analyses of double-Higgs production would allow the upper limits of the two-sided bounds in Eqs. (7) to be tightened. We add that, while the results shown assume $\kappa_\lambda = \kappa_3 = \kappa_4$, the plot remains essentially unchanged if κ_4 is allowed to vary within the range $-10 \lesssim \kappa_4 \lesssim 10$.

The latter feature is also reflected by the red contour in the right panel of Figure 4, which shows the 68% CL region derived from the HEFT calculation of QCD and EW corrections to double-Higgs production presented in this section, applied to LHC Run 2 data. As in the two panels of Figure 1, it is evident that even after including NLO EW corrections involving κ_3 and κ_4 , double-Higgs production shows only a weak dependence on the coupling modifier κ_4 , reflecting the loop suppression of the contribution arising from the Higgs quartic self-coupling. For comparison, the right panel of Figure 4 also displays the 68% CL region from triple-Higgs production, as obtained by the ATLAS collaboration in Ref. [21], shown as a black contour. The constraints on κ_4 from triple-Higgs production are notably stronger than those from double-Higgs production, due to the fact that in $gg \rightarrow HHH$ the Higgs quartic self-coupling already appears at LO in perturbation theory. Finally, note that, in contrast to Figure 1, the constraints on κ_4 from double-Higgs production shown on the right of Figure 4 exhibit a flat direction. This arises because the HEFT results include only terms linear in κ_4 , as evident from Eqs. (34). By contrast, the SMEFT expressions in Eqs. (15) contain κ_4^2 contributions, which break this flat direction. It is important to note that this difference is not related to the choice of SMEFT or HEFT, but rather to whether the square of the one-loop BSM contribution proportional to κ_4 is included.

The NLO EW corrections discussed in this section do not only modify the total double-

Higgs production cross sections but also leave interesting imprints in the kinematic distributions. To illustrate this point, Figure 5 shows the m_{HH} spectra as well as the distributions of the transverse momentum of the leading Higgs boson (p_T^H). The displayed kinematic distributions correspond to the combined ggF and VBF predictions at the LHC with $\sqrt{s} = 14$ TeV for three representative values of κ_λ , assuming again $\kappa_\lambda = \kappa_3 = \kappa_4$. In the SM, i.e., for $\kappa_\lambda = 1$, the m_{HH} spectrum exhibits a peak around 400 GeV. In general, this peak shifts towards smaller m_{HH} values as κ_λ increases. However, larger values of κ_λ can also induce a dip in the spectrum, as illustrated in the upper middle panel for $\kappa_\lambda = 3$. It is further evident that the NLO EW corrections grow in importance with increasing κ_λ and can eventually exceed the size of the QCD corrections around the peak. Furthermore, the NLO EW corrections do not enhance the m_{HH} distribution uniformly, as their impact is more pronounced near the peak. The p_T^H distributions exhibit similar behavior when varying κ_λ . Given the sizable and non-trivial impact of the NLO EW corrections on the kinematic distributions for $\kappa_\lambda \gtrsim 3$, including these effects is expected to improve the sensitivity to κ_3 and κ_4 in an actual LHC data analysis, which necessarily relies on an exclusive phase-space selection.

4 Conclusions

Compared with the Higgs couplings to EW gauge bosons or third-generation fermions, the Higgs self-couplings remain only weakly constrained at LHC Run 2. This leaves substantial room for BSM physics that predominantly modifies the shape of the Higgs potential. In fact, theoretical arguments supported by explicit UV-complete model calculations show that Higgs self-coupling deviations exceeding 200% are still compatible with existing single-Higgs measurements, without requiring fine-tuning of UV parameters [4]. Probing the Higgs self-couplings at the HL-LHC and future colliders via multi-Higgs production therefore explores largely uncharted model and parameter space and provides genuine discovery potential, even if single-Higgs observables show no anomalies.

Fully exploiting the discovery potential of multi-Higgs production channels requires including higher-order perturbative corrections induced by both QCD and EW interactions in the corresponding theoretical predictions. For double-Higgs production, such calculations have been performed in Refs. [23–25] using two consistent EFT approaches. The first two works [23, 24] employed the SMEFT to compute two-loop EW corrections involving the coupling modifiers κ_3 and κ_4 , while the third [25] carried out the calculation within the HEFT framework. We have summarized the main assumptions and results of the SMEFT and HEFT calculations in Sections 2 and 3, respectively. From these discussions, it is clear that the two calculations differ in several conceptual and technical aspects, rendering a direct analytic comparison of the corresponding master formulas in Eqs. (15) and (34) beyond the scope of this note.

For clarity, let us briefly highlight these differences. First, the SMEFT and HEFT are distinct EFTs, with the Higgs being part of an $SU(2)_L$ doublet in the SMEFT and treated as a singlet in the HEFT. This distinction implies, for example, that the Wilson coefficients C_{2n} of the $(\phi^\dagger\phi)^n$ operators in the SMEFT exhibit a different renormalization-group (RG) evolution compared to the coupling modifiers κ_n of the H^n operators in HEFT with $n \geq 3$. The UV structure of the two EFTs is hence not the same. Second, the SMEFT calculation reviewed in Section 2 includes contributions from the Higgs trilinear, quartic, and quintic self-couplings, using Eq. (11) to express κ_5 in terms of κ_3 and κ_4 . The HEFT computations instead include κ_3 and κ_4 while setting $\kappa_5 = 0$. Including corrections from the Higgs quintic self-coupling in the HEFT framework is straightforward, but it would modify the formulas such as Eqs. (30), (32), and (33) presented in Section 3. Third, the two NLO EW calculations retain different orders in the expansion in κ_3 and κ_4 . In the SMEFT computation of Section 2, the square of the two-

loop EW diagrams is included, so the results in Eqs. (15) feature a κ_4^2 dependence. In contrast, the HEFT calculation detailed in Section 3 considers only the interference between the two-loop EW diagrams and the one-loop diagrams, yielding a linear κ_4 dependence in Eqs. (32). The same choice is adopted in the SMEFT calculation of Ref. [24]. However, only for large values of κ_4 — i.e., parameters outside the region where the red and yellow constraints overlap in the plot on the left-hand-side in Figure 1 — does this computation lead to predictions that differ from the parametrization presented in Eqs. (15), which is based on the results obtained in Refs. [23, 48]. In addition, the HEFT calculation of $gg \rightarrow HH$ incorporates terms of $\mathcal{O}(\kappa_3^3)$ and $\mathcal{O}(\kappa_3^4)$, as well as the corrections in Eqs. (27), which are not included in the SMEFT results. Fourth and finally, the phenomenological HEFT results also account for higher-order QCD and EW effects in the VBF double-Higgs production process, whereas the corresponding SMEFT results include only the ggF channel.

Despite these differences, the phenomenological implications of the two calculations are in good agreement. This is illustrated by the constraints in the κ_3 – κ_4 plane derived from LHC Run 2 double-Higgs production data, shown on the left in Figure 1 and on the right in Figure 4, respectively. A more detailed comparison of the SMEFT and HEFT results is presented in Appendix B. In fact, in the parameter region allowed by perturbative unitarity, the two NLO EW computations of double-Higgs production discussed in this note yield numerically similar constraints. This agreement highlights the model-independent complementarity of double- and triple-Higgs production in probing the Higgs potential, with double-Higgs production providing stronger constraints on κ_3 and triple-Higgs production on κ_4 . With the HL-LHC on the horizon and the prospect of future high-energy colliders such as the FCC becoming increasingly tangible, there is a strong motivation to further refine the theoretical description of double-Higgs production. In particular, combining the two NLO EW calculations presented here in a common, systematic framework would facilitate a more robust interpretation of multi-Higgs production measurements at the HL-LHC and future colliders. This task, however, requires significant theoretical work and is therefore left for future research endeavors.

Acknowledgements

The Feynman diagrams in this note were drawn using TikZ-Feynman [74]. This work was carried out within the LHC Higgs Working Group as a contribution to the CERN Report 5. We thank the members of the working group for valuable discussions, and A. Carvalho Antunes de Oliveira, A. Karlberg, G. Landsberg, F. Monti, L. Scyboz and D. Stolarski for their helpful comments, which allowed us to improve the manuscript. The research of J.-L. Ding, H. T. Li, Z. G. Si, J. Wang, X. Zhang, and D. Zhao was supported by the National Natural Science Foundation of China under Grants No. 12321005 and No. 12375076. D. Pagani acknowledges financial support by the MUR through the PRIN2022 Grant 2022EZ3S3F, funded by the European Union — NextGenerationEU.

A Higgs self-couplings and SMEFT operator truncation

In this appendix, we show that restricting the SMEFT Lagrangian to pure Higgs operators of the form $(\phi^\dagger \phi)^n$, as in Eq. (12), is well motivated both phenomenologically and in explicit UV-complete models. Our discussion builds on [75]. The key point is that current constraints from Higgs measurements and EW precision observables (EWPOs) imply a hierarchy among SMEFT Wilson coefficients, such that deviations of the Higgs trilinear self-coupling are dominantly controlled by the operator $(\phi^\dagger \phi)^3$.

Before discussing the SMEFT operators that directly modify the Higgs self-couplings at tree level, it is helpful to first briefly review other effective interactions that can also influence double-Higgs production. Two widely studied dimension-six operators are

$$Q_{\phi G} = (\phi^\dagger \phi) G_{\mu\nu}^a G^{a,\mu\nu}, \quad Q_{\phi t} = (\phi^\dagger \phi) \bar{q} t \tilde{\phi}, \quad (35)$$

where $G_{\mu\nu}^a$ is the QCD field strength tensor, q denotes the left-handed third-generation quark doublet, and we use the shorthand $\tilde{\phi}_i = \epsilon_{ij} (\phi^j)^*$, with ϵ_{ij} the fully antisymmetric Levi-Civita tensor normalized as $\epsilon_{12} = +1$. The first operator induces an effective coupling between the Higgs and gluons, while the second modifies the top-quark Yukawa coupling relative to the SM. Consequently, the operators in Eqs. (35) are also constrained by single-Higgs production and decay. Since the leading single-Higgs production processes are measured with an accuracy of roughly 10%, the Wilson coefficients of $Q_{\phi G}$ and $Q_{\phi t}$ are constrained to be relatively small. These operators contribute to single-Higgs production already at LO, which tightly bounds their size. As a result, their effects on multi-Higgs production are subleading. In the case of triple-Higgs production, this has been demonstrated recently in [76]. Therefore, in analyses such as those presented in Section 2, the contributions of Eqs. (35) and other operators affecting single-Higgs production and decay can be neglected to first approximation.

We now turn to the tree-level matching condition that relates the relevant Wilson coefficients of the dimension-six SMEFT operators to the deviation $\delta\kappa_3$ of the Higgs trilinear self-coupling:

$$\delta\kappa_3 \simeq -\frac{2v^4}{m_h^2} \frac{C_6}{\Lambda^2} + \frac{3v^2}{\Lambda^2} \left(C_{\phi\Box} - \frac{1}{4} C_{\phi D} \right). \quad (36)$$

Here, C_6 is the Wilson coefficient of the dimension-six operator introduced in Eq. (13), while $C_{\phi\Box}$ and $C_{\phi D}$ are the dimensionless Wilson coefficients of

$$Q_{\phi\Box} = (\phi^\dagger \phi) \Box (\phi^\dagger \phi), \quad Q_{\phi D} = (\phi^\dagger D_\mu \phi)^* (\phi^\dagger D^\mu \phi), \quad (37)$$

with $\Box = \partial_\mu \partial^\mu$ denoting the d'Alembert operator.

The first important observation is that the operators in Eq. (37) also induce tree-level contributions to other observables. In particular, the modification $\delta\kappa_V$ of the Higgs coupling to EW gauge bosons and the Peskin-Takeuchi \hat{T} parameter [77] — an important EWPO that measures custodial-symmetry breaking — are given by

$$\delta\kappa_V \simeq \frac{v^2}{\Lambda^2} C_{\phi\Box}, \quad \hat{T} \simeq -\frac{v^2}{2\Lambda^2} C_{\phi D}. \quad (38)$$

In contrast to $\delta\kappa_3$, which is currently only weakly constrained (7), the parameters $\delta\kappa_V$ and \hat{T} are subject to much stronger experimental bounds

$$|\delta\kappa_V| \lesssim 10\%, \quad |\hat{T}| \lesssim 0.1\%, \quad (39)$$

where the limits are taken from [78, 79] and [80, 81], respectively.

Eqs. (36) and (38) can now be used to derive model-independent relations among the Wilson coefficients

$$\frac{|C_6|}{|C_{\phi\Box}|} \simeq \frac{m_h^2}{2v^2} \frac{|\delta\kappa_3|}{|\delta\kappa_V|} \simeq 7, \quad \frac{|C_{\phi\Box}|}{|C_{\phi D}|} \simeq \frac{|\delta\kappa_V|}{2|\hat{T}|} \simeq 50, \quad (40)$$

where for $\delta\kappa_3$ only the contribution of C_6 to Eq. (36) is retained. The numerical values are obtained by adopting the maximal allowed values of $|\delta\kappa_3|$, $|\delta\kappa_V|$, and $|\hat{T}|$ from Eqs. (7) and (39).

The results in Eq. (40) imply that, to satisfy constraints from Higgs measurements and EWPOs, the Wilson coefficients must exhibit a hierarchical structure:

$$|C_6| > |C_{\phi\Box}| \gg |C_{\phi D}|. \quad (41)$$

Kitchen sink BSM scenarios predicting $|C_6| \simeq |C_{\phi\Box}| \simeq |C_{\phi D}| \simeq \mathcal{O}(1)$ are therefore ruled out. Note that the first relation in Eq. (40) also shows that the projected HL-LHC limit of 50% on $\delta\kappa_3$ provides roughly a factor of three less sensitivity than the anticipated 2% HL-LHC measurement of $\delta\kappa_V$ [20].

Realizing the hierarchy (41) within concrete UV-complete scenarios requires some model-building effort. A canonical example is the custodial quadruplet model [4], which naturally allows a large ratio of the Higgs trilinear self-coupling modification relative to other Higgs coupling deviations, while keeping contributions to EWPOs sufficiently suppressed. In this model, the relevant Wilson coefficients are calculable:

$$\frac{C_6}{\Lambda^2} = \frac{2\lambda_\Theta^2}{3M_\Theta^2}, \quad \frac{C_{\phi\Box}}{\Lambda^2} = -\frac{\lambda_\Theta^2}{12\pi^2 M_\Theta^2}, \quad \frac{C_{\phi D}}{\Lambda^2} \simeq -\frac{5g_1^2}{12\pi^2} \ln\left(\frac{M_\Theta}{m_Z}\right) \frac{C_{\phi\Box}}{\Lambda^2}. \quad (42)$$

Here, λ_Θ denotes the coupling of the operator $H^3\Theta$, with Θ the custodial quadruplet, and M_Θ its mass. Eq. (42) shows that the hierarchy (41) is naturally realized because C_6 , $C_{\phi\Box}$, and $C_{\phi D}$ appear at different perturbative orders: C_6 at tree level, $C_{\phi\Box}$ at one loop, and $C_{\phi D}$ at two loops. Note that the expression for $C_{\phi D}$ includes only the leading-logarithmic correction from the one-loop RG evolution of $Q_{\phi\Box}$ into $Q_{\phi D}$ [82], which provides the leading contribution for sufficiently large M_Θ . The loop suppression of $C_{\phi\Box}$ and $C_{\phi D}$ ensures that, for $\delta\kappa_3$ as given in Eq. (36), contributions from the pure Higgs operator Q_6 dominate, so that the relevant physics is well captured by Eq. (12).

The same argument applies to other BSM frameworks that can primarily modify the Higgs potential. Notable examples include the real singlet model with a Z_2 symmetry [83, 84] and the aligned, approximately custodial-symmetric two-Higgs-doublet model with TeV-scale pseudoscalar and charged Higgs masses [85]. In these models, both C_6 and $C_{\phi\Box}$ are generated at one loop, but the matching condition for C_6 depends on higher powers of the quartic scalar couplings than that of $C_{\phi\Box}$. Universal contributions to the Wilson coefficient $C_{\phi D}$ are generated at the two-loop level, as in the custodial quadruplet model. Consequently, in the limit of large quartic scalar couplings a hierarchy of the form (41) emerges, and the correction to the Higgs trilinear self-coupling (36) is fully dominated by Q_6 . Hence, restricting the SMEFT Lagrangian to operators of the form $(\phi^\dagger\phi)^n$, like in Eq. (12), to effectively describe these BSM models is again justified.

We have demonstrated that UV-complete models can realize the phenomenologically required hierarchy (41), in which case truncating the SMEFT Lagrangian as in Eq. (12) provides a reliable approximation. Since the matching between the BSM model and the SMEFT is performed at the high scale set by the masses of the new states, whereas constraints such as those in Figure 1 involve Wilson coefficients evaluated at the EW scale, one must verify that the SMEFT truncation remains valid under the RG evolution. This is indeed the case for the operator Q_6 , which at the one-loop level only mixes into itself [82, 86, 87] and at two loops only into the dimension-six top-quark Yukawa-type operator [5, 88]. In a UV-complete model where Q_6 provides the dominant dimension-six SMEFT deformation, this dominance is thus, to very good approximation, stable under the RG evolution.

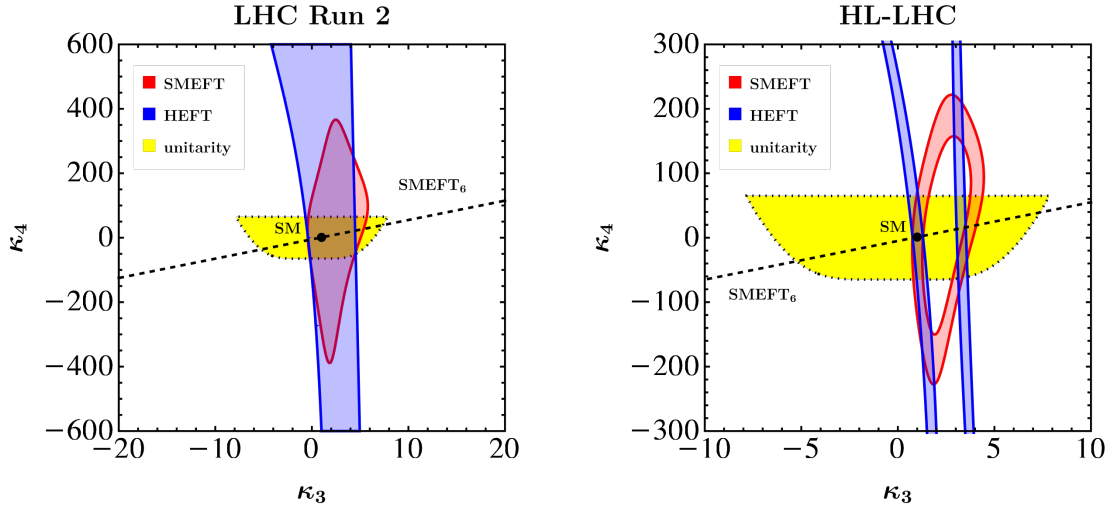


Figure 6: Constraints in the κ_3 – κ_4 plane similar to that shown in Figure 1. The red and blue contours indicate the constraints derived from double-Higgs production in the SMEFT and HEFT, respectively. These constraints are obtained using Eqs. (15) and (34).

B Numerical comparison of SMEFT and HEFT predictions

This appendix provides a more detailed numerical comparison of the SMEFT and HEFT results for double-Higgs production discussed in the main text. Specifically, we compare the phenomenological constraints on κ_3 and κ_4 that follow from Eqs. (15) and (34), respectively, when applied to existing LHC Run 2 data and to hypothetical HL-LHC measurements with an assumed integrated luminosity of 3 ab^{-1} . The results are shown in the two panels of Figure 6, with red and blue contours indicating the constraints derived from double-Higgs production in the SMEFT and HEFT, respectively. These constraints are obtained by requiring $\mu_{2h}^{\text{LHC Run 2}} < 2.9$ [56] and $0.77 < \mu_{2h}^{\text{HL-LHC}} < 1.23$ [57] on the double-Higgs production signal strength at LHC Run 2 and HL-LHC.

For the LHC Run 2 constraints shown on the left in Figure 6, one observes that, within the parameter region allowed by perturbative unitarity — indicated by the yellow areas outlined with black dotted lines — the two NLO EW computations of double-Higgs production discussed in this note yield numerically very similar constraints in the κ_3 – κ_4 plane. The same holds for the region near $\kappa_4 - 1 = 6(\kappa_3 - 1)$, represented by the black dashed line, which corresponds to the relation between κ_3 and κ_4 that arises in the SMEFT at the level of dimension-six operators. For $|\kappa_4| \gtrsim 65$, however, the two constraints begin to deviate. In particular, the HEFT constraint exhibits a flat direction, which arises because the HEFT results include only terms linear in κ_4 , as evident from Eqs. (34). By contrast, the SMEFT expressions in Eqs. (15) contain κ_4^2 contributions, which break this flat direction. Technically, this difference arises because the SMEFT computation in Section 2 includes the square of the two-loop BSM diagrams, while the HEFT calculation in Section 3 considers only their interference with the one-loop SM diagrams.

As shown in the right panel of Figure 6, the impact of κ_4^2 terms on the resulting constraints is even more pronounced in the case that future double-Higgs production measurements yield a two-sided limit on the signal strength, as expected at the HL-LHC. Since the κ_4^2 terms are absent in the HEFT results reported in Eqs. (34), the corresponding constraints now form two bands that are nearly parallel to the κ_4 axis: one passes through the SM point, while the other includes the BSM point $\{\kappa_3, \kappa_4\} \simeq \{3.5, 16\}$. Due to the presence of κ_4^2 terms in Eqs. (15) the SMEFT constraint instead forms an elongated ellipsoidal band. While the global overall

agreement between the SMEFT and HEFT constraints is therefore not particularly strong, one observes that for solutions near the SM point and within the theoretical limits imposed by perturbative unitarity, the SMEFT and HEFT constraints match quite well. A similar behavior is observed in the vicinity of the BSM point $\{\kappa_3, \kappa_4\} \simeq \{3.5, 16\}$, which lies on the line $\kappa_4 - 1 = 6(\kappa_3 - 1)$, corresponding to the parameter space where Q_6 in Eqs. (12) is the only SMEFT operator with a non-zero Wilson coefficient. Here, the agreement between the two constraints is somewhat worse, due to the presence of κ_3^3 and κ_3^4 terms in Eqs. (34) that are absent in Eqs. (15). Including these higher-order terms in Eqs. (15) would noticeably improve the agreement of the constraints near this BSM point. Note that, from a model-building perspective, the parameter space around and between these two points appears particularly relevant, given the hierarchy in Eq. (41) and the fact that, in BSM models such as the custodial quadruplet model discussed in Appendix A that realizes it, one generically expects $|C_8| \simeq |C_6|$. Put differently, BSM models that lead to $|\kappa_4| \gg |\kappa_3|$ appear notoriously difficult to construct — we are not aware of any model that realizes this — implying that the differences between the SMEFT and HEFT constraints shown in Figure 6 are likely of limited phenomenological relevance when confronted with explicit perturbative UV-complete models. We finally note that incorporating kinematic information in double-Higgs production at the HL-LHC is expected to eliminate the solutions near $\{\kappa_3, \kappa_4\} \simeq \{3.5, 16\}$, leaving only SM-like solutions as viable in the κ_3 – κ_4 plane, where the SMEFT and HEFT predictions show rather good agreement.

References

- [1] ATLAS collaboration, G. Aad et al., *Observation of a new particle in the search for the Standard Model Higgs boson with the ATLAS detector at the LHC*, *Phys. Lett. B* **716** (2012) 1–29, [[1207.7214](#)].
- [2] CMS collaboration, S. Chatrchyan et al., *Observation of a New Boson at a Mass of 125 GeV with the CMS Experiment at the LHC*, *Phys. Lett. B* **716** (2012) 30–61, [[1207.7235](#)].
- [3] J. Alison et al., *Higgs boson potential at colliders: Status and perspectives*, *Rev. Phys.* **5** (2020) 100045, [[1910.00012](#)].
- [4] G. Durieux, M. McCullough and E. Salvioni, *Charting the Higgs self-coupling boundaries*, *JHEP* **12** (2022) 148, [[2209.00666](#)].
- [5] M. Gorbahn and U. Haisch, *Indirect probes of the trilinear Higgs coupling: $gg \rightarrow h$ and $h \rightarrow \gamma\gamma$* , *JHEP* **10** (2016) 094, [[1607.03773](#)].
- [6] G. Degrassi, P. P. Giardino, F. Maltoni and D. Pagani, *Probing the Higgs self coupling via single Higgs production at the LHC*, *JHEP* **12** (2016) 080, [[1607.04251](#)].
- [7] W. Bizoń, M. Gorbahn, U. Haisch and G. Zanderighi, *Constraints on the trilinear Higgs coupling from vector boson fusion and associated Higgs production at the LHC*, *JHEP* **07** (2017) 083, [[1610.05771](#)].
- [8] F. Maltoni, D. Pagani, A. Shivaji and X. Zhao, *Trilinear Higgs coupling determination via single-Higgs differential measurements at the LHC*, *Eur. Phys. J. C* **77** (2017) 887, [[1709.08649](#)].
- [9] M. Gorbahn and U. Haisch, *Two-loop amplitudes for Higgs plus jet production involving a modified trilinear Higgs coupling*, *JHEP* **04** (2019) 062, [[1902.05480](#)].

- [10] U. Haisch and G. Koole, *Off-shell Higgs production at the LHC as a probe of the trilinear Higgs coupling*, *JHEP* **02** (2022) 030, [[2111.12589](#)].
- [11] J. Gao, X.-M. Shen, G. Wang, L. L. Yang and B. Zhou, *Probing the Higgs boson trilinear self-coupling through Higgs boson+jet production*, *Phys. Rev. D* **107** (2023) 115017, [[2302.04160](#)].
- [12] U. Haisch and M. Niggetiedt, *Exact two-loop amplitudes for Higgs plus jet production with a cubic Higgs self-coupling*, *JHEP* **10** (2024) 236, [[2408.13186](#)].
- [13] A. Ghosh, M. Griese, U. Haisch and T. H. Park, *Neural simulation-based inference of the Higgs trilinear self-coupling via off-shell Higgs production*, [2507.02032](#).
- [14] ATLAS collaboration, G. Aad et al., *Constraints on the Higgs boson self-coupling from single- and double-Higgs production with the ATLAS detector using pp collisions at $\sqrt{s} = 13$ TeV*, *Phys. Lett. B* **843** (2023) 137745, [[2211.01216](#)].
- [15] CMS collaboration, A. Hayrapetyan et al., *Constraints on the Higgs boson self-coupling from the combination of single and double Higgs boson production in proton-proton collisions at $\sqrt{s} = 13$ TeV*, *Phys. Lett. B* **861** (2025) 139210, [[2407.13554](#)].
- [16] LHC HIGGS CROSS SECTION WORKING GROUP collaboration, A. David, A. Denner, M. Duehrssen, M. Grazzini, C. Grojean, G. Passarino et al., *LHC HXSWG interim recommendations to explore the coupling structure of a Higgs-like particle*, [1209.0040](#).
- [17] LHC HIGGS CROSS SECTION WORKING GROUP collaboration, J. R. Andersen et al., *Handbook of LHC Higgs Cross Sections: 3. Higgs Properties*, [1307.1347](#).
- [18] LHC HIGGS CROSS SECTION WORKING GROUP collaboration, D. de Florian et al., *Handbook of LHC Higgs Cross Sections: 4. Deciphering the Nature of the Higgs Sector*, *CERN Yellow Rep. Monogr.* **2** (2017) 1–869, [[1610.07922](#)].
- [19] ATLAS and CMS collaborations, *Combination of ATLAS and CMS searches for Higgs boson pair production at 13 TeV*, tech. rep., CERN, Geneva, 2025, <https://cds.cern.ch/record/2947512>.
- [20] ATLAS and CMS collaborations, *Highlights of the HL-LHC physics projections by ATLAS and CMS*, tech. rep., CERN, Geneva, 2025, <https://cds.cern.ch/record/2928907>.
- [21] ATLAS collaboration, G. Aad et al., *Search for triple Higgs boson production in the 6b final state using pp collisions at $\sqrt{s} = 13$ TeV with the ATLAS detector*, *Phys. Rev. D* **111** (2025) 032006, [[2411.02040](#)].
- [22] CMS collaboration, *Search for nonresonant triple Higgs boson production in the six b-quark final state in proton-proton collisions at 13 TeV*, tech. rep., CERN, Geneva, 2024, <https://cds.cern.ch/record/2945361>.
- [23] W. Bizoń, U. Haisch and L. Rottoli, *Constraints on the quartic Higgs self-coupling from double-Higgs production at future hadron colliders*, *JHEP* **10** (2019) 267, [[1810.04665](#)].
- [24] S. Borowka, C. Duhr, F. Maltoni, D. Pagani, A. Shivaji and X. Zhao, *Probing the scalar potential via double Higgs boson production at hadron colliders*, *JHEP* **04** (2019) 016, [[1811.12366](#)].
- [25] H. T. Li, Z.-G. Si, J. Wang, X. Zhang and D. Zhao, *Improved constraints on Higgs boson self-couplings with quartic and cubic power dependencies of the cross section*, *Chin. Phys. C* **49** (2025) 023107, [[2407.14716](#)].

- [26] M. Mühlleitner, J. Schlenk and M. Spira, *Top-Yukawa-induced corrections to Higgs pair production*, *JHEP* **10** (2022) 185, [[2207.02524](#)].
- [27] J. Davies, G. Mishima, K. Schönwald, M. Steinhauser and H. Zhang, *Higgs boson contribution to the leading two-loop Yukawa corrections to $gg \rightarrow HH$* , *JHEP* **08** (2022) 259, [[2207.02587](#)].
- [28] J. Davies, K. Schönwald, M. Steinhauser and H. Zhang, *Next-to-leading order electroweak corrections to $gg \rightarrow HH$ and $gg \rightarrow gH$ in the large- m_t limit*, *JHEP* **10** (2023) 033, [[2308.01355](#)].
- [29] H.-Y. Bi, L.-H. Huang, R.-J. Huang, Y.-Q. Ma and H.-M. Yu, *Electroweak Corrections to Double Higgs Production at the LHC*, *Phys. Rev. Lett.* **132** (2024) 231802, [[2311.16963](#)].
- [30] G. Heinrich, S. Jones, M. Kerner, T. Stone and A. Vestner, *Electroweak corrections to Higgs boson pair production: the top-Yukawa and self-coupling contributions*, *JHEP* **11** (2024) 040, [[2407.04653](#)].
- [31] J. Davies, K. Schönwald, M. Steinhauser and H. Zhang, *Electroweak corrections to $gg \rightarrow HH$: Factorizable contributions*, in *Loops and Legs in Quantum Field Theory*, 7, 2024, [2407.05787](#).
- [32] M. Bonetti, P. Rendler and W. J. Torres Bobadilla, *Two-loop light-quark Electroweak corrections to Higgs boson pair production in gluon fusion*, *JHEP* **07** (2025) 024, [[2503.16620](#)].
- [33] A. Bhattacharya, F. Campanario, S. Carlotti, J. Chang, J. Mazzitelli, M. Mühlleitner, J. Ronca and M. Spira, *Higgs-Pair Production via Gluon Fusion: Top-Yukawa- and light-quark-induced electroweak Corrections*, [2512.14823](#).
- [34] F. Maltoni, D. Pagani and X. Zhao, *Constraining the Higgs self-couplings at e^+e^- colliders*, *JHEP* **07** (2018) 087, [[1802.07616](#)].
- [35] T. Liu, K.-F. Lyu, J. Ren and H. X. Zhu, *Probing the quartic Higgs boson self-interaction*, *Phys. Rev. D* **98** (2018) 093004, [[1803.04359](#)].
- [36] M. Chiesa, F. Maltoni, L. Mantani, B. Mele, F. Piccinini and X. Zhao, *Measuring the quartic Higgs self-coupling at a multi-TeV muon collider*, *JHEP* **09** (2020) 098, [[2003.13628](#)].
- [37] M. Gonzalez-Lopez, M. J. Herrero and P. Martinez-Suarez, *Testing anomalous $H - W$ couplings and Higgs self-couplings via double and triple Higgs production at e^+e^- colliders*, *Eur. Phys. J. C* **81** (2021) 260, [[2011.13915](#)].
- [38] P. Stylianou and G. Weiglein, *Constraints on the trilinear and quartic Higgs couplings from triple Higgs production at the LHC and beyond*, *Eur. Phys. J. C* **84** (2024) 366, [[2312.04646](#)].
- [39] A. Papaefstathiou and G. Tetlalmatzi-Xolocotzi, *Multi-Higgs boson production with anomalous interactions at current and future proton colliders*, *JHEP* **06** (2024) 124, [[2312.13562](#)].
- [40] H. Abouabid et al., *HHH whitepaper*, *Eur. Phys. J. C* **84** (2024) 1183, [[2407.03015](#)].
- [41] Z. Dong, X. Sun, B. Guo, L. Zhang, Z. Li, J. Wang et al., *Probing triple Higgs production via $4\tau 2b$ decay channel at a 100 TeV hadron collider*, *JHEP* **08** (2025) 040, [[2504.04037](#)].

- [42] S. Alioli, P. Nason, C. Oleari and E. Re, *A general framework for implementing NLO calculations in shower Monte Carlo programs: the POWHEG BOX*, *JHEP* **06** (2010) 043, [[1002.2581](#)].
- [43] S. Borowka, N. Greiner, G. Heinrich, S. P. Jones, M. Kerner, J. Schlenk et al., *Full top quark mass dependence in Higgs boson pair production at NLO*, *JHEP* **10** (2016) 107, [[1608.04798](#)].
- [44] S. Borowka, N. Greiner, G. Heinrich, S. P. Jones, M. Kerner, J. Schlenk et al., *Higgs Boson Pair Production in Gluon Fusion at Next-to-Leading Order with Full Top-Quark Mass Dependence*, *Phys. Rev. Lett.* **117** (2016) 012001, [[1604.06447](#)].
- [45] G. Heinrich, S. P. Jones, M. Kerner, G. Luisoni and E. Vryonidou, *NLO predictions for Higgs boson pair production with full top quark mass dependence matched to parton showers*, *JHEP* **08** (2017) 088, [[1703.09252](#)].
- [46] G. Heinrich, S. P. Jones, M. Kerner, G. Luisoni and L. Scyboz, *Probing the trilinear Higgs boson coupling in di-Higgs production at NLO QCD including parton shower effects*, *JHEP* **06** (2019) 066, [[1903.08137](#)].
- [47] E. Bagnaschi, G. Degrossi and R. Gröber, *Higgs boson pair production at NLO in the POWHEG approach and the top quark mass uncertainties*, *Eur. Phys. J. C* **83** (2023) 1054, [[2309.10525](#)].
- [48] W. Bizoń, U. Haisch, L. Rottoli, Z. Gillis, B. Moser and P. Windischhofer, *Addendum to: Constraints on the quartic Higgs self-coupling from double-Higgs production at future hadron colliders* [*JHEP* **10** (2019) 267], *JHEP* **02** (2024) 170, [[2402.03463](#)].
- [49] M. Grazzini, G. Heinrich, S. Jones, S. Kallweit, M. Kerner, J. M. Lindert et al., *Higgs boson pair production at NNLO with top quark mass effects*, *JHEP* **05** (2018) 059, [[1803.02463](#)].
- [50] S. Amoroso et al., *Les Houches 2019: Physics at TeV Colliders: Standard Model Working Group Report*, in *11th Les Houches Workshop on Physics at TeV Colliders: PhysTeV Les Houches*, 3, 2020, [2003.01700](#).
- [51] J. Baglio, F. Campanario, S. Glaus, M. Mühlleitner, J. Ronca and M. Spira, *$gg \rightarrow HH$: Combined uncertainties*, *Phys. Rev. D* **103** (2021) 056002, [[2008.11626](#)].
- [52] J. Butterworth et al., *PDF4LHC recommendations for LHC Run II*, *J. Phys. G* **43** (2016) 023001, [[1510.03865](#)].
- [53] U. Haisch, A. Sankar and G. Zanderighi, *A new probe of the quartic Higgs self-coupling*, [2505.20463](#).
- [54] J. Alwall, R. Frederix, S. Frixione, V. Hirschi, F. Maltoni, O. Mattelaer et al., *The automated computation of tree-level and next-to-leading order differential cross sections, and their matching to parton shower simulations*, *JHEP* **07** (2014) 079, [[1405.0301](#)].
- [55] F. Maltoni, E. Vryonidou and M. Zaro, *Top-quark mass effects in double and triple Higgs production in gluon-gluon fusion at NLO*, *JHEP* **11** (2014) 079, [[1408.6542](#)].
- [56] ATLAS collaboration, G. Aad et al., *Combination of Searches for Higgs Boson Pair Production in pp Collisions at $\sqrt{s} = 13$ TeV with the ATLAS Detector*, *Phys. Rev. Lett.* **133** (2024) 101801, [[2406.09971](#)].

- [57] ATLAS collaboration, *Projected sensitivity of Higgs boson pair production combining the $b\bar{b}\gamma\gamma$ and $b\bar{b}\tau^+\tau^-$ final states with the ATLAS detector at the HL-LHC*, tech. rep., CERN, Geneva, 2022, <https://cds.cern.ch/record/2798448>.
- [58] ATLAS collaboration, *HL-LHC prospects for the measurement of triple-Higgs production in the $6b$ final state at the ATLAS experiment*, tech. rep., CERN, Geneva, 2025, <https://cds.cern.ch/record/2924772>.
- [59] L. Di Luzio, R. Gröber and M. Spannowsky, *Maxi-sizing the trilinear Higgs self-coupling: how large could it be?*, *Eur. Phys. J. C* **77** (2017) 788, [[1704.02311](#)].
- [60] OPENLOOPS 2 collaboration, F. Buccioni, J.-N. Lang, J. M. Lindert, P. Maierhöfer, S. Pozzorini, H. Zhang et al., *OpenLoops 2*, *Eur. Phys. J. C* **79** (2019) 866, [[1907.13071](#)].
- [61] F. Buccioni, S. Pozzorini and M. Zoller, *On-the-fly reduction of open loops*, *Eur. Phys. J. C* **78** (2018) 70, [[1710.11452](#)].
- [62] S. Catani and M. H. Seymour, *A General algorithm for calculating jet cross-sections in NLO QCD*, *Nucl. Phys. B* **485** (1997) 291–419, [[hep-ph/9605323](#)].
- [63] T. Gleisberg and F. Krauss, *Automating dipole subtraction for QCD NLO calculations*, *Eur. Phys. J. C* **53** (2008) 501–523, [[0709.2881](#)].
- [64] J. Davies, G. Mishima, K. Schönwald and M. Steinhauser, *Analytic approximations of $2 \rightarrow 2$ processes with massive internal particles*, *JHEP* **06** (2023) 063, [[2302.01356](#)].
- [65] B. Jäger, A. Karlberg and S. Reinhardt, *Precision tools for the simulation of double-Higgs production via vector-boson fusion*, *JHEP* **06** (2025) 022, [[2502.09112](#)].
- [66] J. Davies, K. Schönwald, M. Steinhauser and D. Stremmer, *ggxy: a flexible library to compute gluon-induced cross sections*, [2506.04323](#).
- [67] G. Buchalla, O. Catà and C. Krause, *Complete Electroweak Chiral Lagrangian with a Light Higgs at NLO*, *Nucl. Phys. B* **880** (2014) 552–573, [[1307.5017](#)].
- [68] X. Liu, Y.-Q. Ma and C.-Y. Wang, *A Systematic and Efficient Method to Compute Multi-loop Master Integrals*, *Phys. Lett. B* **779** (2018) 353–357, [[1711.09572](#)].
- [69] X. Liu and Y.-Q. Ma, *AMFlow: A Mathematica package for Feynman integrals computation via auxiliary mass flow*, *Comput. Phys. Commun.* **283** (2023) 108565, [[2201.11669](#)].
- [70] M. Cacciari, F. A. Dreyer, A. Karlberg, G. P. Salam and G. Zanderighi, *Fully Differential Vector-Boson-Fusion Higgs Production at Next-to-Next-to-Leading Order*, *Phys. Rev. Lett.* **115** (2015) 082002, [[1506.02660](#)].
- [71] F. A. Dreyer and A. Karlberg, *Vector-Boson Fusion Higgs Production at Three Loops in QCD*, *Phys. Rev. Lett.* **117** (2016) 072001, [[1606.00840](#)].
- [72] F. A. Dreyer and A. Karlberg, *Fully differential Vector-Boson Fusion Higgs Pair Production at Next-to-Next-to-Leading Order*, *Phys. Rev. D* **99** (2019) 074028, [[1811.07918](#)].
- [73] F. A. Dreyer, A. Karlberg and L. Tancredi, *On the impact of non-factorisable corrections in VBF single and double Higgs production*, *JHEP* **10** (2020) 131, [[2005.11334](#)].
- [74] J. Ellis, *TikZ-Feynman: Feynman diagrams with TikZ*, *Comput. Phys. Commun.* **210** (2017) 103–123, [[1601.05437](#)].

- [75] U. Haisch, (2026), *The potential of the Higgs @ FCC*, Talk given at the 9th FCC Physics workshop, Max Planck Institute for Physics.
- [76] L. Panizzi, *The role of the top Yukawa coupling in triple Higgs production at the LHC*, 2512.03003.
- [77] M. E. Peskin and T. Takeuchi, *A New constraint on a strongly interacting Higgs sector*, Phys. Rev. Lett. **65**, 964 (1990), doi:[10.1103/PhysRevLett.65.964](https://doi.org/10.1103/PhysRevLett.65.964).
- [78] ATLAS collaboration, *Combined measurements of Higgs boson production and decay at $\sqrt{s} = 13$ TeV using up to 140 fb^{-1} of data collected by the ATLAS Experiment*, tech. rep., CERN, Geneva, 2025, <https://cds.cern.ch/record/2937634>.
- [79] CMS collaboration, A. Hayrapetyan *et al.*, *Combined measurements and interpretations of Higgs boson production and decay in proton-proton collisions at $\sqrt{s} = 13$ TeV*, 2602.18611.
- [80] S. Schael *et al.*, *Precision electroweak measurements on the Z resonance*, Phys. Rept. **427**, 257 (2006), doi:[10.1016/j.physrep.2005.12.006](https://doi.org/10.1016/j.physrep.2005.12.006), [[hep-ex/0509008](https://arxiv.org/abs/hep-ex/0509008)].
- [81] S. Navas *et al.*, *Review of particle physics*, Phys. Rev. D **110**(3), 030001 (2024), doi:[10.1103/PhysRevD.110.030001](https://doi.org/10.1103/PhysRevD.110.030001).
- [82] R. Alonso, E. E. Jenkins, A. V. Manohar and M. Trott, *Renormalization Group Evolution of the Standard Model Dimension Six Operators III: Gauge Coupling Dependence and Phenomenology*, JHEP **04**, 159 (2014), doi:[10.1007/JHEP04\(2014\)159](https://doi.org/10.1007/JHEP04(2014)159), [[1312.2014](https://arxiv.org/abs/1312.2014)].
- [83] U. Haisch, M. Ruhdorfer, E. Salvioni, E. Venturini and A. Weiler, *Singlet night in Feynman-ville: one-loop matching of a real scalar*, JHEP **04**, 164 (2020), doi:[10.1007/JHEP04\(2020\)164](https://doi.org/10.1007/JHEP04(2020)164), [Erratum: JHEP **07**, 066 (2020)], [[2003.05936](https://arxiv.org/abs/2003.05936)].
- [84] V. Maura, B. A. Stefanek and T. You, *Accuracy complements energy: electroweak precision tests at Tera-Z*, JHEP **10**, 022 (2025), doi:[10.1007/JHEP10\(2025\)022](https://doi.org/10.1007/JHEP10(2025)022), [[2412.14241](https://arxiv.org/abs/2412.14241)].
- [85] H. Bahl, J. Braathen and G. Weiglein, *New Constraints on Extended Higgs Sectors from the Trilinear Higgs Coupling*, Phys. Rev. Lett. **129**(23), 231802 (2022), doi:[10.1103/PhysRevLett.129.231802](https://doi.org/10.1103/PhysRevLett.129.231802), [[2202.03453](https://arxiv.org/abs/2202.03453)].
- [86] E. E. Jenkins, A. V. Manohar and M. Trott, *Renormalization Group Evolution of the Standard Model Dimension Six Operators I: Formalism and lambda Dependence*, JHEP **10**, 087 (2013), doi:[10.1007/JHEP10\(2013\)087](https://doi.org/10.1007/JHEP10(2013)087), [[1308.2627](https://arxiv.org/abs/1308.2627)].
- [87] E. E. Jenkins, A. V. Manohar and M. Trott, *Renormalization Group Evolution of the Standard Model Dimension Six Operators II: Yukawa Dependence*, JHEP **01**, 035 (2014), doi:[10.1007/JHEP01\(2014\)035](https://doi.org/10.1007/JHEP01(2014)035), [[1310.4838](https://arxiv.org/abs/1310.4838)].
- [88] L. Born, J. Fuentes-Martín and A. E. Thomsen, *Next-to-Leading Order Running in the SMEFT*, 2601.19974.